Available online at www.sciencedirect.com
SCIENCE DIRECT®
Surface Science 547 (2003) 85–98
SURFACE SCIENCE
www.elsevier.com/locate/susc

Adsorption and diffusion energetics of hydrogen atoms on Fe(1 1 0) from first principles

D.E. Jiang, Emily A. Carter *

Department of Chemistry and Biochemistry, Box 951569, University of California, Los Angeles, CA 90095-1569, USA

Received 10 August 2003; accepted for publication 4 October 2003

Abstract

Spin-polarized density functional theory (DFT) has been used to characterize hydrogen atom adsorption and diffusion energetics on the Fe(1 1 0) surface. The Kohn-Sham equations are solved with periodic boundary conditions and within the all-electron projector-augmented-wave (PAW) formalism, using a generalized gradient approximation (GGA) to account for electron exchange and correlation. We investigate the site preference of H on Fe(1 1 0) for 0.25, 0.50, and 1.0 ML coverages and find that the quasi three-fold site is the only stable minimum (in agreement with experiment). We find the long and short bridge sites to be transition states for H diffusion on Fe(1 1 0), while the on top site is a rank-2 saddle point. The preference of the three-fold site is rationalized via an analysis of the site- and orbital-resolved density of states. An analysis of charge density differences suggests that the H–Fe interaction is quite covalent, with only ~0.1 electron transferred from Fe atoms to H in the three-fold site of Fe(1 1 0). We also compare two experimentally observed 0.50 ML phases for H/Fe(1 1 0): a graphitic (2×2)-2H and a (2×1) phase. We confirm the LEED data that the Fe(1 1 0)-(2×2)-2H superstructure is more stable at low temperature. The predicted adsorption structure and weak substrate reconstruction for the Fe(1 1 0)-(2×2)-2H phase roughly agree with experiment, though discrepancies do exist regarding the H-surface height and the H–H distance. Moreover, trends in work function with coverage are predicted to be qualitatively different than older measurements, with even the sign of the work function changes in question. Lastly, a zig–zag diffusion path for H atoms on Fe(1 1 0) is proposed, involving a very low (<0.2 eV) barrier.

Keywords: Density functional calculations; Chemisorption; Iron; Hydrogen atom; Surface diffusion

1. Introduction

The interaction of hydrogen with transition metal surfaces is of great fundamental and practical interest in both heterogeneous catalysis and metallurgy. Transition metal surfaces catalyze numerous hydrogenation reactions. Hydrogen chemisorption on iron is particularly important, not only as a reactant in Fe-catalyzed ammonia synthesis [1], the Fischer–Tropsch reaction [2] (and many others), but also because hydrogen is known to embrittle steels [3,4], causing fracture and ultimately failure of the steel component.

The adsorption of hydrogen on low-index Fe surfaces has been investigated experimentally for

* Corresponding author. Tel.: +1-310-206-5118; fax: +1-310-267-0319.
E-mail address: eac@chem.ucla.edu (E.A. Carter).

0039-6028/$ - see front matter © 2003 Elsevier B.V. All rights reserved.
doi:10.1016/j.susc.2003.10.007

more than 25 years [5–9]. Molecular hydrogen is found to adsorb dissociatively on these surfaces and the process is strongly exothermic. The following survey of the literature focuses only on the adsorption of H on the Fe(1 1 0) surface, which is the closest-packed surface of body-centered-cubic (bcc) Fe (α-Fe). Fig. 1 displays four high-symmetry sites on Fe(1 1 0): the long bridge (LB), the quasi three-fold (TF), the short bridge (SB), and the on-top (OT) sites.

The experimental picture of H adsorption on Fe(1 1 0) is now rather clear. Early low energy electron diffraction (LEED) experiments at temperatures above 140 K by Bozso et al. [5] revealed a (2×1) phase for $\theta_H = 1/2$ ML and a (3×1)-2H phase for $\theta_H = 2/3$ ML. For both phases, the adatoms originally were proposed to reside at the long bridge (LB) sites, though the authors did not provide quantitative structural analysis at that time. Later, however, Moritz et al. (from the same research group) concluded [9] that hydrogen adsorbs at the quasi three-fold (TF) site in both the (2×1) and the (3×1)-2H phases. More recent low temperature LEED studies by Nichtl-Pecher et al. [10] and Hammer et al. [11] confirmed this TF site occupancy. They also found at $\theta_H = 1/2$ ML that a new graphitic (2×2)-2H phase forms at 35 K, concomitant with a weak substrate reconstruction induced by H adsorption. Moreover, they observed that this (2×2)-2H phase transforms reversibly upon heating to the (2×1) phase at 80 K.

Despite the clear identification of the H adsorption site on Fe(1 1 0) from LEED, numerous theoretical studies have provided contradictory conclusions about the H site occupancy [12–18]. This is no doubt due to the diversity of approximations used in the models. By embedding a cluster of Fe and H atoms represented by muffin tin potentials at the surface of jellium, Muscat [14], in 1982, calculated the one-electron energy change of moving H from the free electron surface to the Fe cluster surface and concluded that H prefers the TF site over the LB site. For an H–Fe bond length of 1.78 Å, the model predicted the (2×1) phase to be stable, while for an H–Fe bond length of 1.59 Å, the model predicted a graphitic (2×2)-2H structure to be favored. Subsequent LEED experiments [11] did find the new (2×2)-2H phase, but with a much longer H–Fe bond of 1.84 Å. In 1983, Muscat used the same method to explore the occupancy of the SB site by H, then concluding that the SB site is the most favorable. Raeker and DePristo [16] studied H chemsorption on Fe(1 1 0) using the semi-empirical corrected effective medium theory with a periodic slab model. They suggested that the LB site was the most stable, but with the TF and SB sites only 0.01 and 0.05 eV less stable, respectively. A recent study by Cremaschi et al. [17], using a limited configuration interaction (CI) calculation with an embedded cluster-in-cluster model, found the LB site to be the most stable, with the SB and TF sites only 0.03 and 0.05 eV less stable than the LB site, respectively. Clearly, all of these studies suggest that all three bridging sites are close in energy.

Density-functional studies of H adsorption on Fe(1 1 0) have been rare. The only one we have found is by Eder et al. [19], who studied the oxidation of Fe(1 0 0) and Fe(1 1 0) by H_2O using spin-polarized periodic density functional theory (DFT) with a slab model. Studying only the 1/4 ML case, they found that H prefers the TF site, followed by the LB site, the SB site, and the OT site. They used ultrasoft pseudopotentials (US-PPs) and the GGA exchange–correlation functional of Perdew et al. (PW91) [20]. However, it is known that US-PPs are less reliable for magnetic systems such as Fe [21] and that PW91 tends to overbind adsorbates on metal surfaces [22]. Therefore, we have revisited and extended earlier work on H/Fe(1 1 0), using periodic DFT within an all-electron formalism and an exchange–correlation functional (see Section 2) that, taken together, better describe magnetic systems and adsorption

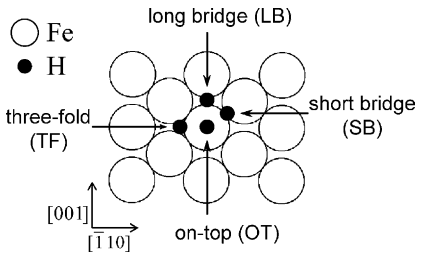

Fig. 1. High symmetry adsorption sites on Fe(1 1 0).

energetics, with a goal to resolve the discrepancies among early theoretical studies (and experiment). Moreover, in Eder et al.'s work and other earlier theoretical studies, the hydrogen coverage was limited to 0.25 ML or below and the nature of the various high-symmetry sites, i.e., whether a site is minimum or a saddle point, was not determined. We extend earlier work by examining the full coverage range and by determining the nature of critical points on the potential energy surface, in order to compare with experiment and to provide a reference point for further simulations of surface diffusion and H-embrittlement of iron.

The paper is organized as follows. In Section 2, we present the theoretical method employed. Results for the clean Fe(1 1 0) surface are presented in Section 3.1. We then compare the energy of H adsorption on various sites for $\theta_H = 1/4$ and 1 ML in Section 3.2. Section 3.3 offers a comparison of the (2×2)-2H and (2×1) phases formed at $\theta_H = 1/2$ ML. In Section 3.4, we show how the work function and charge distribution change with coverage. We discuss our results in Section 4 and conclude in Section 5.

2. Theoretical method

The first-principles calculations performed are based on spin-polarized DFT [23,24]. The Vienna Ab Initio Simulation Package (VASP) is used to solve the Kohn-Sham equations with periodic boundary conditions and a plane-wave basis set [25,26]. Here we employ Blöchl's projector augmented wave (PAW) method [27] as implemented by Kresse and Joubert [21]. The PAW method is an all-electron DFT technique (within the frozen core approximation) with the computational efficiency of pseudopotential DFT algorithms. As mentioned above, its use is necessary for accurate calculations of certain transition metals, which are sometimes poorly described by US-PPs. For the treatment of electron exchange and correlation, it is well known that the generalized gradient approximation (GGA) is needed to give an accurate description of magnetic properties and energetics of bulk Fe phases [28]. Therefore, all calculations are done with the GGA functional of Perdew et al. (PW91) [20], using the one-electron quantities (partial waves, projectors, etc.) supplied with VASP that are required to construct the self-consistent PAW potential. (We use the standard version of the PAW–GGA potentials for Fe and H.) While the PW91 GGA functional yields reliable optimized geometries, PW91 tends to overbind adsorbates on metal surfaces [22]. We therefore also present results employing the RPBE GGA exchange–correlation functional [22], which slightly modifies the exchange part of the PBE functional [29]. RPBE appears to give a better description of atomization energies of molecules and adsorption energetics. We therefore use the PW91 functional for all geometry optimizations, and report the energetics for relaxed structures from both PW91 and RPBE. The spin interpolation of the correlation energy is accomplished by using the Vosko–Wilk–Nusair method [30].

We use a kinetic energy cutoff of 400 eV, which we find is sufficient to converge the total energies of ferromagnetic (FM) bcc Fe and isolated atomic H to within 2 meV/atom. The Monkhorst-Pack scheme [31] is used for the k-point sampling. Using a $15\times15\times15$ k-mesh, we obtain the equilibrium lattice constant, bulk modulus, and local magnetic moment for ferromagnetic bcc Fe. The results agree very well with previous PAW–GGA calculations and experiment (Table 1). Placing an H_2 molecule in a 10 Å cubic box, we obtain its equilibrium bond length, bond dissociation energy, and harmonic vibrational frequency (Table 2). The agreement with previous PAW–GGA calculations and experiment is also quite reasonable.

In order to obtain a thick enough slab to represent the Fe(1 1 0) surface, we performed

Table 1
Equilibrium lattice constant (a), bulk modulus (B), and magnetic moment (M) of ferromagnetic bcc Fe using PAW–GGA (PW91) DFT

Method	a (Å)	B (GPa)	M (μ_B)
Present PAW	2.834	174	2.21
PAW[a]	2.83	174	2.20
Experiment	2.86[b]	168[c]	2.22[c]

[a] Ref. [32].
[b] Extrapolated to 0 K, Ref. [33].
[c] Ref. [34].

Table 2
Bond length (r_e), dissociation energy (D_e), and vibrational frequency (v) of H_2 using PAW–GGA (PW91) DFT

Method	r_e (Å)	D_e (eV)	v (cm^{-1})
Present PAW	0.752	4.56	4300
PAW[a]	0.75	4.58	4300
Experiment[b]	0.741	4.75	4401

[a] Ref. [35].
[b] Ref. [36].

convergence tests of the number of slab layers, vacuum thickness, and the k-point sampling for the bulk-terminated surface. The surface primitive cell is used, with the energy of the unrelaxed surface used as the criterion for convergence. The results are shown in Table 3. It can be seen that a $14\times14\times1$ k-mesh, seven slab layers, and 10 Å vacuum converges the unrelaxed surface energy to within 1 mJ m^{-2}. We therefore use those parameters for the surface primitive cell, while a $7\times7\times1$ k-mesh is used for the (2×2) surface cell.

The first order Methfessel–Paxton method [37] is used for the Fermi surface smearing, with a width of 0.1 eV in order to obtain accurate forces. A conjugate gradient or quasi-Newton algorithm is employed to relax the ionic positions to the ground state geometry. When the maximum force acting on each atom of the slab drops below 0.01 eV/Å, the structural relaxation is stopped. Only the top three layers of the seven slab layers are allowed to relax. The bottom four layers are kept fixed in bulk positions to represent the semi-infinite bulk crystal beneath the surface. (Residual forces on the fourth layer atoms are also <0.01 eV/Å.) Hydrogen adsorbs on top of the seven Fe layers and is allowed to relax together with the top three Fe layers.

Table 3
The unrelaxed surface energy (γ) of the Fe(1 1 0) slab as a function of slab and vacuum thickness and k-point sampling, using PAW–GGA (PW91) DFT

k-mesh	Number of layers in slab	Vacuum (Å)	γ (J m^{-2})
$8\times8\times1$	5	10	2.367
$10\times10\times1$	5	10	2.430
$12\times12\times1$	5	10	2.442
$14\times14\times1$	5	10	2.429
$16\times16\times1$	5	10	2.430
$12\times12\times1$	7	10	2.437
$12\times12\times1$	9	10	2.436
$12\times12\times1$	5	8	2.441
$12\times12\times1$	5	12	2.442

The work function is obtained from the difference between the vacuum energy level (given as the value where the electrostatic potential is constant in the middle of the vacuum region) and the Fermi level. Vibrational frequencies of H on the high-symmetry sites are determined by diagonalizing a finite difference construction of the Hessian matrix with displacements of 0.01 Å (only allowing H to move). The site-projected and orbital-resolved density of states are done using a quick projection scheme that does not require Wigner-Seitz radius inputs and works only for PAW potentials, but not for US-PPs or norm-conserving pseudopotentials [38].

3. Results

3.1. Clean Fe(1 1 0)

Fe(1 1 0) is the closest-packed surface of bcc Fe. It has been studied [39] in greater detail very recently with the same plane-wave code using ultrasoft pseudo-potentials (US-PP) and the GGA for the exchange–correlation energy. Both experiment [40,41] and recent DFT studies [32,39,42] show that Fe(1 1 0) is basically bulk-terminated, with only very small relaxation and no reconstruction. We compare our results about the relaxation of the Fe(1 1 0) surface with recent DFT studies and experiment in Table 4. Due to the small magnitude of the relaxation, the surface energy of Fe(1 1 0) is basically unchanged after relaxation. Our results are nearly identical to the previous PAW results by Stibor et al. [32] for the interlayer relaxation and the magnetic moment for the surface Fe atoms, except for $\Delta_{1,2}$. This may be due to their use of a different kinetic energy cutoff and a smaller k-mesh ($8\times8\times1$). The agreement between our results and previous US-PP results is generally very good for interlayer relaxation, with our PAW prediction for the surface energy closer to the experimental value. In fact, all the predictions are within experimental

Table 4
Interlayer relaxation ($\Delta_{i,i+1}$), magnetic moment of surface Fe atoms (M), and surface energy (γ) for Fe(1 1 0) using PAW–GGA (PW91) DFT

Method	$\Delta_{1,2}$ (%)[a]	$\Delta_{2,3}$ (%)	$\Delta_{3,4}$ (%)	$M(\mu_B)$	γ (J m^{-2})
Present PAW	−0.36	+0.46	−0.26	2.58	2.43
PAW[b]	−0.08	+0.40	−0.25	2.59	–
US-PP[c]	−0.33	+0.26	−0.06	–	2.27
US-PP[d]	−0.35	+0.44	–	2.74	2.29
Exp.	$+0.5 \pm 2.0$[e]	$+0.5 \pm 1.0$[f]	–	–	2.41[g]

[a] $\Delta_{i,i+1}$ is defined as the percentage change of interlayer spacing between substrate layer i and $i+1$, compared with the bulk spacing d_0. Layer 1 is the topmost substrate layer.
[b] Ref. [32].
[c] Ref. [39].
[d] Ref. [42].
[e] Ref. [40].
[f] Ref. [41].
[g] Ref. [43].

error. The good agreement between the PAW data and experiment for the Fe(1 1 0) surface give us confidence to go on to study H adsorption with this method.

3.2. H adsorption on the relaxed Fe(1 1 0) surface at $\theta_H = 1/4$ and 1 ML

Table 5 shows the adsorption energy, the H-surface distance, and the distance from H to its nearest Fe neighbor at $\theta_H = 1/4$ and 1 ML after the structure of the H/Fe(1 1 0) slab is relaxed. For all coverages examined, the TF site is found to be the lowest in energy, in agreement with experiment. Our predictions of the H-surface bond length and the H–Fe distance for the TF site also concur with experiment. By calculating the frequency spectrum of the H adatom on a fixed Fe substrate, we find that only the TF site is a true minimum at either coverage. The LB and SB sites are transition states for H diffusion on Fe(1 1 0), with one imaginary frequency for both coverages. By contrast, the OT site is actually not a minimum nor a transition state at either coverage, but is a rank-2 saddle point with two imaginary frequencies. At 1/4 ML coverage, the LB transition state is 0.05 eV higher in energy than the TF site, while the SB transition state is 0.19 eV higher, suggesting a very low barrier to diffusion of H atoms on Fe(1 1 0). The OT higher-order saddle point lies 0.72 eV higher than the TF site minimum. At 1 ML coverage, the energies of the LB, SB, and OT sites relative to the TF site are 0.14, 0.26, and 0.96 eV, respectively. Thus, the energy differences between the TF site and the other sites increase with coverage, presumably due to increasing repulsions (discussed later) between coadsorbed hydrogen. We see that the OT site is significantly higher in energy than the other sites at both coverages, while the TF, LB, and SB sites are all very close in energy, especially for $\theta_H = 1/4$ ML.

Earlier theoretical predictions are also given in Table 5. Eder et al.'s periodic DFT-GGA (PW91) calculations using US-PPs yielded similar results to ours [19] at $\theta_H = 1/4$ ML. Ab initio CI embedded cluster calculations of Cremaschi et al. [17], modeling the asymptotic limit of zero coverage, predicted that the LB site is most stable, followed by the SB, TF, and OT sites. Again, the LB, SB, and TF sites are all predicted to be very close in energy, with the OT site again being strongly disfavored. Qualitatively, all theory predicts the OT to be strongly disfavored at all coverages, while all other sites lie fairly close in energy. The slab calculations are just able to resolve the right ground state (TF), whereas the embedded cluster-in-cluster model has a slight error.

Experimental H_2 adsorption energies and vibrational frequencies of the H-surface bond on Fe(1 1 0) are available for comparison. Room temperature electron energy loss spectroscopy (EELS) of H_2 adsorption on Fe(1 1 0) at a coverage ~0.25 ML by Baro and Erley [45] shows an H-surface symmetric stretch frequency at 1060 cm^{-1},

Table 5
H atom adsorption energy ($E_{ad} = E_{H/Fe\text{-}slab} - E_{Fe\text{-}slab} - E_H$) without zero point energy corrections, energy difference between sites relative to the TF site (ΔE), H-surface distance ($d_{H\text{–}S}$), and the distance from H to the nearest Fe ($d_{H\text{–}Fe}$) at $\theta_H = 1$ and 1/4 ML from PAW–GGA (PW91) DFT

	Site	E_{ad} (eV/atom)	ΔE (eV)[a]	$d_{H\text{–}S}$ (Å)	$d_{H\text{–}Fe}$ (Å)	Site nature
Experiment	TF	−2.86[b]	–	0.9 ± 0.1[c]	1.75 ± 0.05[c]	–
Present work	TF	−3.00 (−2.83)	0 (0)	0.94	1.78	Minimum
1/4 ML	LB	−2.95 (−2.80)	0.05 (0.03)	0.95	1.74	Transition state
	SB	−2.81 (−2.66)	0.19 (0.15)	1.14	1.69	Transition state
	OT	−2.28 (−2.12)	0.72 (0.71)	1.56	1.56	Rank-2 saddle point
PW91-GGA/	TF	–	0	0.95	–	–
USPP Ref. [19]	LB	–	0.06	0.94	–	–
1/4 ML[a]	SB	–	0.18	1.16	–	–
	OT	–	0.75	1.52	–	–
CI embedded	TF	−2.71	0	0.87	1.74	–
cluster Ref. [17]	LB	−2.76	−0.05	0.89	1.69	–
<0.1 ML	SB	−2.73	−0.02	1.03	1.61	–
	OT	−2.33	0.38	1.36	1.36	–
Present work	TF	−2.91 (−2.76)	0 (0)	0.90	1.72	Minimum
1 ML	LB	−2.77 (−2.62)	0.14 (0.16)	0.92	1.69	Transition state
	SB	−2.65 (−2.48)	0.26 (0.28)	1.13	1.67	Transition state
	OT	−1.95 (−1.80)	0.96 (0.96)	1.53	1.53	Rank-2 saddle point

Values for E_{ad} using the RPBE GGA exchange–correlation functional are shown in parentheses.

[a] Adsorption energy relative to the TF site.

[b] An experimental heat of adsorption (ΔH_{exp}) of -1.05 ± 0.10 eV/H_2 for $\theta_H = 0.22$–0.45 ML [44] and an experimental D_e of H_2 (4.75 eV/H_2) [36] are used to obtain this value. The zero point energy contributions to ΔH_{exp} were removed by using the theoretical vibrational frequencies.

[c] Ref. [9]. LEED value for $\theta_H = 1/2$ ML. See Table 6 for our work on $\theta_H = 1/2$ ML.

in excellent agreement with our calculation of 1063 cm^{-1} for 1/4 ML coverage. Temperature programmed desorption of H_2 from H/Fe(1 1 0) by Kurz and Hudson [44] yields a heat of adsorption (ΔH, negative values mean exothermic) of -1.05 ± 0.10 eV/H_2 for $\theta_H = 0.22$–0.45 ML and a temperature range of 200–500 K. After accounting for zero point energy corrections, we obtain a (PW91) heat of adsorption of −1.39 eV/H_2 for $\theta_H = 1/4$ ML for H on the TF site, about 30% larger than experiment. Eder et al. [19] also obtained too high a ΔH (−1.38 eV/H_2) with PW91 for $\theta_H = 1/4$ ML. This overbinding of atoms and small molecules to transition metal surfaces is believed to be a deficiency of the PW91 functional [22]. Looking back at Table 5, we see that the RPBE functional reduces the adsorption energies for $\theta_H = 1/4$ ML. RPBE gives the same site stability trend as PW91, but it systemically lowers the binding of H to the surface by ~0.16 eV for H atom adsorption. Converting the H atom adsorption energy to the heat of adsorption and including H_2 and H_{ad} zero point energy corrections, RPBE GGA yields −1.06 eV/H_2 for the heat of adsorption of H_2 onto two TF sites, in excellent agreement with experiment.

3.3. $\theta_H = 1/2$ ML phases

As mentioned earlier, recent low temperature (35 K) LEED studies by Nichtl-Pecher et al. [10] and Hammer et al. [11] confirmed that H resides in the TF site and gave evidence for a new (2×2)-2H superstructure with a graphitic arrangement of adatoms, which reversibly transforms to the well-known (2×1) phase at a critical temperature of about 80 K. In both superstructures, hydrogen induces a weak substrate reconstruction. The top

view of the two structures is shown Fig. 2. Here we use the names for the two superstructures from early experimental studies, but we note that the (2×1) structure and the (2×2)-2H structure are named using different primitive surface lattice vectors of Fe(1 1 0), as shown by the arrows in Fig. 2. The (2×1) structure can transform to the (2×2)-2H structure simply by moving to the left the H atom (small solid circle in Fig. 2) at the center of the (2×2) supercell (the rhombus in Fig. 2(a)) to the nearest neighbor TF site.

We compare the energies of these two configurations in Table 6. We find, as in experiments below 80 K, that the (2×2)-2H phase is slightly more stable than the (2×1) phase, although the energy difference is very small (~0.015 eV/H); smaller than the likely errors in the theory. This small energy difference is reflected in the nearly identical H-surface distances for both phases. Small differences are predicted for the H–Fe distances in each phase: H is almost equidistant to the three closest Fe atoms in the (2×2)-2H structure, while in the (2×1) structure H is closer to two of the Fe atoms by 0.02 Å (toward the LB site). Although the relaxation in the Fe substrate is small for both systems, we find a lower energy is achieved for (2×2)-2H structure by a slightly higher coordination of Fe atoms around H.

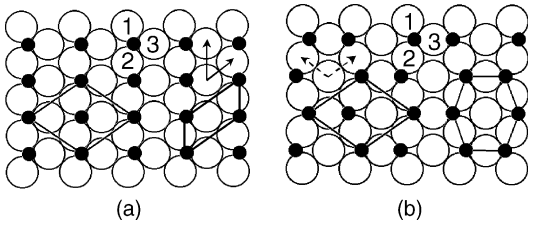

Fig. 2. $\theta_H = 0.5$ ML adsorption structures of H (solid circles) on Fe(1 1 0) (open circles): (a) the (2×1) phase and (b) the (2×2)-2H phase. The hexagonal (graphitic) unit cell of the (2×2)-2H phase is shown in (b).

The LEED study of the (2×2)-2H phase indicates that the substrate undergoes a weak reconstruction and that H atoms move away significantly from the normal TF site towards the LB site. We compare the structural details of the relaxed (2×2)-2H phase with experiment in Fig. 3 and Table 7. The top and side views of the structure proposed by the low temperature LEED data are shown in Fig. 3(a) and (b), respectively. The two most striking features proposed by Hammer et al. [11] are: (i) the movement (depicted by the top arrows in Fig. 3(b)) of H atoms toward the LB site by 0.18 Å from the ideal TF site (for H in the ideal TF site of the experimental model, Hy = 1.52 Å) and (ii) the buckling of the substrate layers. From the 0.18 Å shift to the LB site, the authors reasoned that only the strongly H-coordinated Fe atoms (hatched in Fig. 3(a)) are induced to rearrange. These Fe atoms are pushed toward the bulk. They also suggested a weaker buckling among weakly coordinated Fe atoms (unshaded in Fig. 3(a)) might occur, but they did not check that possibility. Moreover, they proposed a buckling in the second substrate layer.

By contrast with the experimental model of this (2×2)-2H phase, we find that H only moves about 0.01 Å towards the LB site in our relaxed structure (for H in the ideal TF site of our supercell, Hy = 1.50 Å). In addition, H is almost equidistant to the three Fe atoms closely coordinated to it (Table 6), which means all the three Fe atoms [unshaded atoms and diagonally hatched atoms in Fig. 3(c)] are strongly coordinated to the hydrogen. We do find that these strongly coordinated Fe atoms are pushed towards the bulk, compared with those Fe atoms not directly coordinated to H [horizontally hatched in Fig. 3(c)]. This agress with Hammer et al.'s observation. However, no buckling among those strongly coordinated Fe atoms is found in the present work.

Table 6
PAW–GGA–DFT (PW91) H atom adsorption energies ($E_{ad} = E_{H/Fe\text{-}slab} - E_{Fe\text{-}slab} - E_H$), H-surface distances ($d_{H\text{–}S}$), the distances from H to the nearest Fe atoms ($d_{H\text{–}Fe}$) at $\theta_H = 1/2$ ML for the (2×2)-2H and (2×1) configurations

Structure	E_{ad} (eV/atom)	$d_{H\text{–}Fe1}$ (Å)	$d_{H\text{–}Fe2}$ (Å)	$d_{H\text{–}Fe3}$ (Å)	$d_{H\text{–}S}$ (Å)
(2×2)-2H	−3.016 (−2.851)	1.774	1.773	1.779	0.938
(2×1)	−3.001 (−2.840)	1.770	1.770	1.799	0.939

E_{ad} from the RPBE GGA exchange–correlation functional are shown in parentheses.

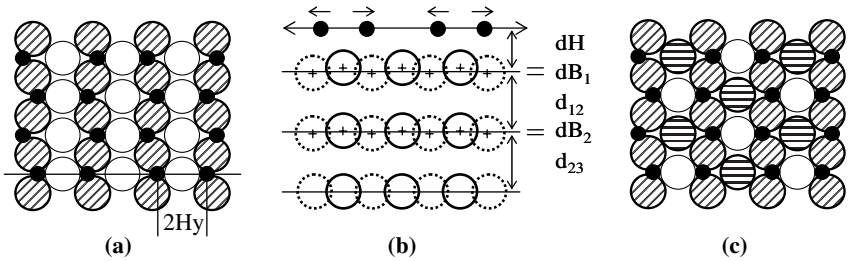

Fig. 3. Substrate reconstruction of the Fe(1 1 0)-(2×2)-2H phase: (a) experimental model (top view, 2Hy is the distance between two H atoms); (b) structural parameters (side view): H-surface height (dH), interlayer spacings (d_{12} and d_{23}), and intralayer bucklings (dB_1 and dB_2). The top arrows indicate the direction of the movement of H off ideal threefold positions; (c) theoretical model from this work. The distinctions between various types of surface Fe atoms are explained in the text. In the experimental model (a), dB_1 is the difference in height between hatched and unshaded Fe atoms, while in our theoretical model (c), dB_1 is the difference in height between weakly coordinated (horizontally shaded) and strongly coordinated (diagonally shaded and unshaded) Fe atoms.

Table 7
Comparison of the predicted [PAW–GGA (PW91)] structure of the structurally relaxed (2×2)-2H phase with experiment

	dH (Å)	d_{H-Fe} (Å)	Hy (Å)	dB_1 (Å)	$\Delta_{1,2}$ (%)[a]	dB_2 (Å)	$\Delta_{2,3}$ (%)[a]
This work	0.93	1.77	1.51	0.016	0.15	0	0.89
Exp. [11]	1.11 ± 0.2	1.84 ± 0.35	1.70 ± 0.33	0.04 ± 0.025	0 ± 2	0.02 ± 0.015	1 ± 3

See Fig. 3 for definitions of distances reported here.
[a] $\Delta_{i,i+1}$ is defined as the same in Table 4.

Another significant difference between our relaxed structure and the one proposed by Hammer et al. for (2×2)-2H is the H-surface distance. In our opinion, the experimental value of 1.11 Å is too large. The (2×2)-2H phase transforms reversibly to (2×1) phase around 80 K. We expect the height of H adsorbed on the surface should not change much between these two phases. Our calculations show that the difference in height is actually very small (~0.001 Å) between the (2×2)-2H and the (2×1) phases (Table 6). However, the H-surface height from the experiment model of the (2×2)-2H phase is ~0.20 Å larger than that of (2×1), which has a H-surface height of 0.90 ± 0.10 Å [9].

In principle, anharmonicity in vibrations can change the average positions of atoms and may account for the difference between our zero Kelvin DFT predictions and measurements at finite temperature. If the potential energy surface is very flat, this indeed could be important. However, we find quite high frequencies for the frustrated translations of H on Fe(1 1 0): 740 cm^{-1} for the normal mode along [$\bar{1}$ 1 0] and 954 cm^{-1} for the normal mode along [0 0 1] for the (2×2)-2H phase, within the constraint of a fixed Fe substrate. Since these frequencies are high, the harmonic approximation applies; we therefore expect the average position of each H will be close to the equilibrium position at low temperatures. The LEED experiment for the (2×2)-2H phase to which we are comparing was performed at 35 K. At this temperature, thermal effects on the vibrational energies are expected to be very small. We therefore are justified in comparing our DFT results directly with the low-temperature LEED measurements.

Although the structural parameters (Fig. 3(b) and Table 7) from our calculations are all within the experimental error bars (except for dB_2), we suggest that our relaxed structure of the (2×2)-2H configuration is distinct from what Hammer et al. proposed. Future experiments may resolve this discrepancy.

3.4. Coverage dependent properties: adsorption energy, work function change, and charge distribution

Table 8 displays how several physical properties of H in the TF site change with coverage. The coverage dependence of the adsorption energy is

Table 8
The adsorption energy (E_{ad}), work function change relative to pure Fe(1 1 0) ($\Delta\Phi$), electron transfer to H (Δn), and surface dipole (μ) for different coverages of H in the TF site

θ_H	Structure	E_{ad} (eV/H)	$\Delta\Phi$ (eV)	Δn (e^-)	μ (D)
1	(1×1)	−2.91	0.023	0.09	0
0.5	(2×1)	−3.00	0.027	0.11	0.022
0.5	(2×2)-2H	−3.02	0.077	0.11	0.038
0.25	(2×2)	−3.00	0.022	0.12	0.029

indicative of the nature of the interaction between adsorbed H atoms. Examining the adsorption energies for the (1×1), (2×1), and (2×2) structures, we see that the adsorption energy increases slightly as the coverage is reduced. We interpret this to mean a small repulsion exists between H atoms in the (1×1) structure, ~0.045 eV per pair of H atoms, with negligible repulsion for $\theta_H = 1/2$ and 1/4 ML.

We obtain a work function of 4.73 eV for the pure Fe(1 1 0) slab, in agreement with the experimental value of 4.5–4.70 eV for polycrystalline Fe [46,47]. Single crystal work function measurements for Fe(1 1 0) are not available for comparison. After adsorption of H, we find the work function increases by ~0.025 eV for the (1×1), (2×1), and (2×2) structures. The (2×2)-2H structure shows a significantly larger increase of ~0.077 eV. The only experimental measurements (in 1977 by Bozso et al. [5]) suggest instead that the work function *decreases* upon H_2 adsorption by ~0.020–0.085 eV in the coverage range 0.25–1 ML. No other experiments have confirmed this decrease. We also examined the work function change for the other adsorption sites (LB, SB, and OT) of H on Fe(1 1 0). They all show a positive change, though the magnitude of the change varies from site to site. Given the discrepancy between theory and experiment regarding even the sign of the work function change, we suggest further measurements are warranted. It is true that work function values calculated by periodic DFT may depend strongly on the vacuum thickness, *k*-point sampling, and slab thickness [35]; however it is likely that coverage trends utilizing a constant set of parameters are reliable.

The change in work function after H adsorption is due to charge rearrangement, which in turn induces a surface dipole moment that affects the work function. We have calculated the charge density differences

$$\Delta\rho = \rho_{H/Fe\text{-}slab} - \rho_{Fe\text{-}slab} - \rho_H,$$

where $\rho_{H/Fe\text{-}slab}$, $\rho_{Fe\text{-}slab}$, and ρ_H are the charge densities for the H/Fe(1 1 0) slab, the clean Fe(1 1 0) slab, and an isolated H layer (in the same positions as the adsorbed H's), respectively. We find a charge transfer of only 0.09–0.12 electrons from Fe to H, by integrating $\Delta\rho$ around the H atom with a radius of 0.90 Å, suggesting rather covalent metal-H bonding. (Changing this rather arbitrary radius by ±0.20 Å causes only ~0.02 e changes in the extent of charge transfer.) The amount of the charge transfer is basically the same for $\theta_H = 0.25$ and 0.50 ML.

By integrating $\Delta\rho$ over planes of constant height over the surface along the surface normal (defined as the *z*-axis here), we obtain the change in charge density upon adsorption as a function of *z*, the distance into the vacuum from the Fe surface layer:

$$\Delta\rho(z) = \int \Delta\rho(x,y,z)\,dx\,dy.$$

For $\theta_H = 0.25$ and 0.50 ML, the $\Delta\rho(z)$ vs *z* plots are almost identical, so Fig. 4 only displays results for the (1×1) and (2×2)-2H phases. A small amount of charge depletion from surface Fe atoms and accumulation on H adatoms evident. We see that the charge depletion is slightly less at the surface plane ($z = 0$) for $\theta_H = 0.50$ ML. The charge depletion on the vacuum side of the H atom is due to a slight shift in the center of mass of the charge density on the H adatom towards the surface, again consistent with primarily covalent bonding.

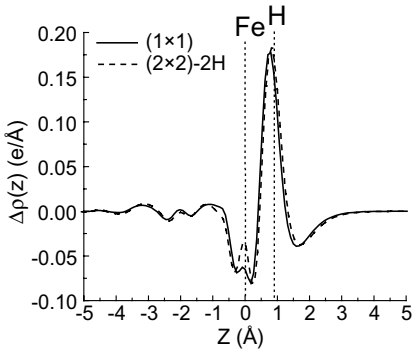

Fig. 4. Valence charge density difference integrated for planes parallel to the surface, as a function of the distance from the topmost substrate layer ($z = 0$) for H in the TF site of Fe(1 1 0).

The change in work function is determined by the induced surface dipole moment μ, which is defined as

$$\mu = \int \Delta\rho(z) z \, dz.$$

Here we find that the contributions to the surface dipole from charge transfer to H and from depletion in the vacuum region cancel each other, resulting in a very small work function change. This cancellation is almost perfect for $\theta_H = 1$ ML, while not so complete for the (2×2)-2H structure ($\theta_H = 0.50$ ML). The calculated trend for the surface dipole agrees with that of the work function change for $\theta_H = 0.5$ and 0.25 ML. It is likely that as θ_H increases, the Fe-H bonding becomes even more covalent, in order to minimize dipole-dipole repulsions. This may account for the complete lack of a surface dipole for $\theta_H = 1$ ML. The shorter H-surface bond length (Table 5) for $\theta_H = 1$ ML than for $\theta_H = 1/4$ ML also supports this point.

4. Discussion

Recent and more accurate experimental structure determinations [10,11] clearly show that H prefers the TF site on the Fe(1 1 0) surface. Our calculations confirm this assignment. However, it would be useful to determine why hydrogen, or any atomic adsorbate for that matter, prefers high coordination sites on metal surfaces, while many molecular adsorbates do not [1]. The higher coordination number and the interaction of metal orbitals with the H 1s orbital have both been invoked to explain the preference of hollow sites on the low-index surfaces of metals [26,48]. The site preference in bulk Fe also offers a correlation. Theoretical studies by us [49] and others [50–52] and experiment [53] all show that H prefers the tetrahedral site in bulk Fe. When the crystal is cut to form the (1 1 0) surface, the tetrahedral site in the bulk becomes the TF site on the surface. In order to investigate the preference of the TF site further, we compare here the orbital-resolved local density of states and charge density differences for the OT site and the TF site. We will argue that the ease of bonding to interstitial electrons [54–56] leads to the stability of the TF site.

Fig. 5 shows the orbital-resolved local density of states (LDOS) for an adsorbed H atom and a surface Fe atom for the TF site and the OT site at $\theta_H = 1$ ML. We see that the H 1s band of the TF site is peaked mostly between −5.0 and −6.0 eV below E_F, while the corresponding band for the OT site is much broader and is centered around −3.0 eV below E_F. When H is placed on the TF site, the H 1s band has a strong interaction with Fe sp band, as seen by the significant (multi-eV) shift of the Fe 4s and $4p_x$ LDOS for the TF site compared to the bare Fe surface. The OT site shows no such shifts in the 4s and 4p states. The H 1s band of the TF site also has some interactions with the Fe 3d bands that have x components, i.e., $3d_{xy}$, $3d_{x^2-y^2}$ and $3d_{xz}$. By contrast, the only stabilizing shift observed when H adsorbs in the OT site is that of the Fe $3d_{z^2}$ band, suggesting the OT site forms a σ-bond to the H via the d_{z^2} orbital on Fe. Given the largest shift for H in the TF site involves the 4sp electrons on Fe, we conclude that the TF site surface Fe atoms mainly utilize 4sp electrons to bond to H, with smaller contributions from the 3d electrons. This is consistent with simple bonding picture where hollow site adsorption mainly utilizes more delocalized interstitial electrons of sp character [54–57], while on top adsorption, because of its more localized nature, involves the localized d-orbitals. For σ-bonds, such as to H,

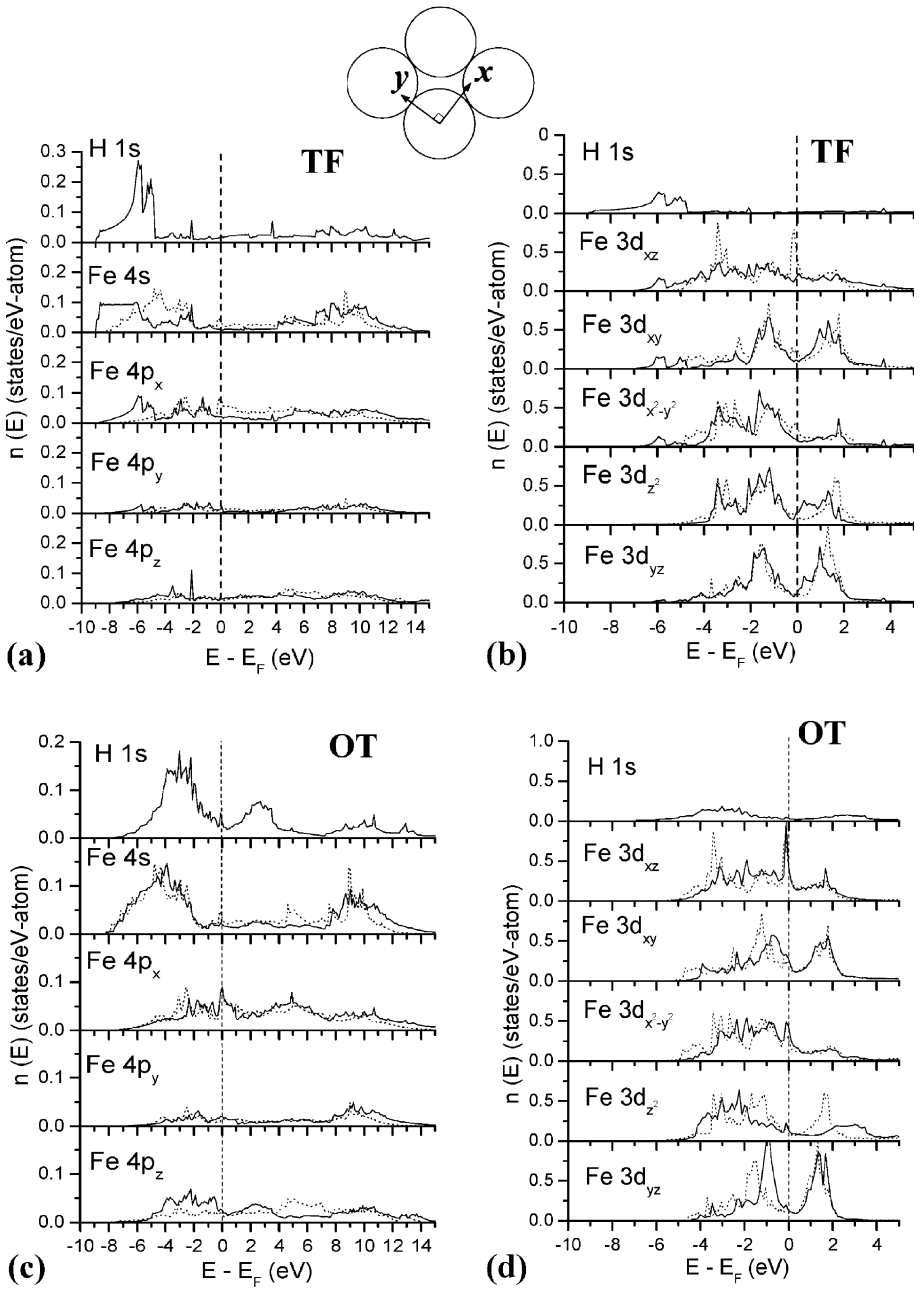

Fig. 5. Site-projected and orbital-resolved local density of states (LDOS) for adsorbed H and surface Fe atoms of H/Fe(1 1 0) for $\theta_H = 1$ ML: (a, b) H on the three-fold site; (c, d) H on the on-top site. LDOS for pure Fe(1 1 0) surface atoms are shown in dotted curves. The direction of surface normal is the *z*-axis, and an Fe(1 1 0) surface primitive cell, the associated *x*-axis and *y*-axis, and the position of the TF site are as shown. Note scales are consistent within each panel, but differ between panels.

this dictates use of a d_{z^2} orbital on Fe in the OT site.

Fig. 6 shows two charge density slices of pure Fe(1 1 0). The OT site has a much larger density

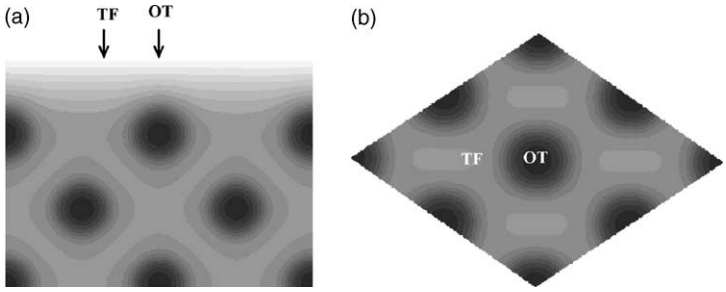

Fig. 6. Valence charge density of pure Fe(1 1 0): (a) side view from [0 0 1]; (b) top view at the surface Fe layer. Charge-density isoplanes drawn in the range of 0.01 (white) to 8.5 (black) e/Å^3 on a logarithmatic scale. Fe nuclei are at the centers of the darkest regions.

gradient compared to the TF site. Now suppose we adsorb an H atom onto the Fe surface. Given our discussions earlier that suggest a primarily covalent Fe–H bond, we imagine H will prefer a site able to provide approximately one electron that can pair up with the H electron to form this covalent bond. We investigated the TF and OT sites from this point of view, by evaluating approximately the "number of electrons" associated with each site. This is accomplished by centering a sphere at the midpoint between the H and the surface Fe layer, where the sphere was given a radius of half the H–Fe bond length. Then we calculate how many electrons are contained in this sphere for the pure Fe surface. We obtain 0.63 e for the TF site and 1.87 e for the OT site, where the latter suggests the Fe $3d_{z^2}$ orbital is nearly doubly occupied and therefore less able to effectively participate in covalent bonding. We conclude that H prefers the TF site because there is $\sim$1 electron associated with the TF site already set up to form a covalent bond to the unpaired H 1s electron. This idea that adsorbates bond to the interstitial electrons was proposed earlier by Goddard and coworkers for adsorption on surfaces of fcc metals [58].

The present study provides a basic picture of H adsorption on the Fe(1 1 0) surface, which further allows us to speculate about thermally activated paths for H diffusion on the Fe(1 1 0) surface and into bulk Fe. Recall from Section 3.2 that the SB and LB sites are transition states for surface diffusion, while the OT site is not. We therefore focus on diffusion via the bridge sites only. Using $\theta_H = 1/4$ ML adsorption energy data for our discussion, we estimate barriers for H diffusion from

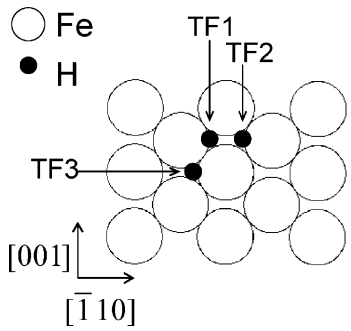

Fig. 7. Three-fold sites on Fe(1 1 0) considered for surface diffusion of H.

TF 1 to TF 2 and TF 3 (Fig. 7) to be 0.05 eV via the LB site to TF 2 and 0.19 eV via the SB site to TF 3. The extremely small barrier via the LB site provides an easily accessible way for H to oscillate between two nearest-neighbor TF sites. For longer-range diffusion, one likely path would be via the SB site with a barrier of 0.19 eV, following a zig–zag pattern across the surface as it hops from TF site to TF site via SB sites. H will avoid the OT site, which, as already noted, is a much-higher energy rank-2 saddle point.

Quantum diffusion is also possible for H on Fe(1 1 0). Gomer and coworkers [59,60] studied atomic H diffusion on W(1 1 0) using a field-emission-fluctuation method and observed clear transitions from thermally activated diffusion to a quantum diffusion regime. They also proposed the SB site as the transition state and a zig–zag diffusion mechanism. Using scanning tunneling microscopy (STM), Lauhon and Ho [61] recently reported the first STM images of isolated hydro-

gen atoms on a metal surface and a similar classical to quantum diffusion transition for H/Cu(1 1 0). Classical diffusion barriers were deduced from the measured thermal diffusion coefficients in those studies. Analogous experiments for H/Fe(1 1 0) have not yet been done, but could determine the transition temperature from the thermally activated diffusion to the quantum diffusion regime and could be used to verify our predictions of the H diffusion barriers.

Fe is one of those metals in which H diffuses very quickly [62], though its solubility in Fe is very low. We find that H diffuses in bulk bcc Fe between tetrahedral sites along the [1 1 0] direction with a tiny diffusion barrier of only 0.042 eV [49]. A channel of tetrahedral sites along the surface normal exists just under the TF site. Consequently, we believe that the first step for H diffusion into bulk Fe from the (1 1 0) surface will involve H moving from the TF site directly down to the nearest tetrahedral site just beneath the surface Fe layer. Calculations are underway to test this idea.

5. Conclusions

Employing first principles PAW–DFT–GGA techniques, we have studied atomic H adsorption on Fe(1 1 0). In agreement with experiment, we find that the quasi three-fold (TF) site is the only stable minimum for coverages between 1/4 and 1 ML. By contrast, the long bridge site, short bridge site, and on-top site are all found to be saddle points rather than true minima, in contrast to suggestions by earlier theoretical work. Previous studies did not evaluate the frequency spectrum (Hessian matrix) to determine the nature of the critical points. Our work illustrates the importance of doing so. The long and short bridge sites are true transition states for H diffusion on Fe(1 1 0) (with both barriers < 0.2 eV), while the on-top site is a high energy rank-2 saddle point. For long-range diffusion, we propose a zig–zag path over short-bridge sites as the likely means to diffuse from TF site to TF site across the surface. In terms of quantitative results, we find that the RPBE GGA exchange–correlation functional can correct the 30% (!) overbinding by PW91 of adsorbed H on Fe(1 1 0), yielding a heat of adsorption of 1.06 eV/H_2, in excellent agreement with experiment.

We also confirmed the experimental finding that the (2×2)-2H configuration is (slightly) more stable than the (2×1) configuration and that a small substrate reconstruction occurs. However, two discrepancies emerge between our predictions and experiment [11] concerning the structure of the (2×2)-2H phase. We find the H-surface height to be 0.93 Å, while the measured value is 1.11 ± 0.20 Å; our work shows that H basically stays at the ideal threefold site, while the experimental analysis indicates that H moves toward the long bridge site by $\sim$0.20 Å.

We find that the work function *increases* slightly after H adsorbs on Fe(1 1 0) surface, in direct contradiction to rather old experiments that suggested a slight decrease in work function after H adsorption. The bonding between H and the Fe surface is found by several means to be quite covalent, involving primarily the Fe 4sp electrons that localize in the TF sites. Very small lateral repulsions are found at high coverage. Overall, structures and relative stabilities agree with experiment, suggesting that follow-up studies of bulk penetration and diffusion, where less experimental data are available, can be pursued with some degree of confidence with this level of theory.

Acknowledgements

We thank the Army Research Office and the Department of Defense Multidisciplinary University Research Initiative (DOD-MURI) for funding this research. We thank the Maui High Performance Computing Center and the NAVO Major Shared Resources Center for providing CPU time.

References

[1] G.A. Somorjai, Introduction to Surface Chemistry and Catalysis, John Wiley & Sons, New York, 1994.
[2] R.B. Anderson, The Fischer–Tropsch Synthesis, Academic Press, Orlando, Fla, 1984.
[3] W. Zhong, Y. Cai, D. Tomanek, Nature (London, United Kingdom) 362 (1993) 435.
[4] J.-S. Wang, Eng. Fract. Mech. 68 (2001) 647.

[5] F. Bozso, G. Ertl, M. Grunze, M. Weiss, Appl. Surf. Sci. 1 (1977) 103.
[6] M. Weiss, G. Ertl, F. Nitschke, Appl. Surf. Sci. 2 (1979) 614.
[7] K. Yoshida, Jpn. J. Appl. Phys. 19 (1980) 1873.
[8] R. Imbihl, R.J. Behm, K. Christmann, G. Ertl, T. Matsushima, Surf. Sci. 117 (1982) 257.
[9] W. Moritz, R. Imbihl, R.J. Behm, G. Ertl, T. Matsushima, J. Chem. Phys. 83 (1985) 1959.
[10] W. Nichtl-Pecher, J. Gossmann, L. Hammer, K. Heinz, K. Müller, J. Vac. Sci. Tech. A 10 (1992) 501.
[11] L. Hammer, H. Landskron, W. Nichtl-Pecher, A. Fricke, K. Heinz, K. Müller, Phys. Rev. B 47 (1993) 15969.
[12] K. Binder, W. Kinzel, D.P. Landau, Surf. Sci. 117 (1982) 232.
[13] W. Kinzel, W. Selke, K. Binder, Surf. Sci. 121 (1982) 13.
[14] J.P. Muscat, Surf. Sci. 118 (1982) 321.
[15] R.W. Pasco, P.J. Ficalora, Surf. Sci. 134 (1983) 476.
[16] T.J. Raeker, A.E. DePristo, Surf. Sci. 235 (1990) 84.
[17] P. Cremaschi, H. Yang, J.L. Whitten, Surf. Sci. 330 (1995) 255.
[18] A. Juan, R. Hoffmann, Surf. Sci. 421 (1999) 1.
[19] M. Eder, K. Terakura, J. Hafner, Phys. Rev. B. 6411 (2001) 115426.
[20] J.P. Perdew, J.A. Chevary, S.H. Vosko, K.A. Jackson, M.R. Pederson, D.J. Singh, C. Fiolhais, Phys. Rev. B 46 (1992) 6671.
[21] G. Kresse, D. Joubert, Phys. Rev. B 59 (1999) 1758.
[22] B. Hammer, L.B. Hansen, J.K. Nørskov, Phys. Rev. B 59 (1999) 7413.
[23] P. Hohenberg, W. Kohn, Phys. Rev. 136 (1964) B864.
[24] W. Kohn, L.J. Sham, Phys. Rev. 140 (1965) A1133.
[25] G. Kresse, J. Hafner, Phys. Rev. B 48 (1993) 13115.
[26] A. Eichler, J. Hafner, G. Kresse, J. Phys.: Condens. Matter 8 (1996) 7659.
[27] P.E. Blöchl, Phys. Rev. B 50 (1994) 17953.
[28] D.J. Singh, W.E. Pickett, H. Krakauer, Phys. Rev. B 43 (1991) 11628.
[29] J.P. Perdew, K. Burke, M. Ernzerhof, Phys. Rev. Lett. 77 (1996) 3865.
[30] S.H. Vosko, L. Wilk, M. Nusair, Can. J. Phys. 58 (1980) 1200.
[31] H.J. Monkhorst, J.D. Pack, Phys. Rev. B 13 (1976) 5188.
[32] A. Stibor, G. Kresse, A. Eichler, J. Hafner, Surf. Sci. 507–510 (2002) 99.
[33] M. Acet, H. Zaehres, E.F. Wassermann, W. Pepperhoff, Phys. Rev. B. 49 (1994) 6012.
[34] C. Kittel, Introduction to Solid State Physics, 7th ed., John Wiley & Sons, New York, 1996.
[35] G. Kresse, J. Hafner, Surf. Sci. 459 (2000) 287.
[36] K.P. Huber, G. Herzberg, Molecular Spectra and Molecular Structure 4: Constants of Diatomic Molecules, Van Norstrand Reinhold Co., New York, 1979.
[37] M. Methfessel, A.T. Paxton, Phys. Rev. B 40 (1989) 3616.
[38] G. Kresse, J. Furthmüller, VASP the Guide. Available from <http://cms.mip.univie.ac.at/VASP/>.
[39] M.J.S. Spencer, A. Hung, I.K. Snook, I. Yarovsky, Surf. Sci. 513 (2002) 389.
[40] H.D. Shih, F. Jona, U. Bardi, P.M. Marcus, J. Phys. C: Solid State Phys. 13 (1980) 3801.
[41] C. Xu, D.J. O'Connor, Nucl. Instr. Meth. Phys. Res., Sec. B: Beam Inter. Mater. Atom. B 53 (1991) 315.
[42] A. Arya, E.A. Carter, J. Chem. Phys. 118 (2003) 8982.
[43] W.R. Tyson, W.A. Miller, Surf. Sci. 62 (1977) 267.
[44] E.A. Kurz, J.B. Hudson, Surf. Sci. 195 (1988) 15.
[45] A.M. Baro, W. Erley, Surf. Sci. 112 (1981) L759.
[46] D.E. Eastman, Phys. Rev. B. 2 (1970) 1.
[47] A. Cardell, Phys. Rev. 92 (1953) 554.
[48] M.H. Cohen, M.V. Ganduglia-Pirovano, J. Kudrnovsky, Phys. Rev. Lett. 72 (1994) 3222.
[49] D.E. Jiang, E.A. Carter, to be submitted.
[50] R. Griessen, Phys. Rev. B 38 (1988) 3690.
[51] C. Minot, C. Demangeat, J. Chem. Phys. 86 (1987) 2161.
[52] P. Nordlander, J.K. Nørskov, F. Besenbacher, J. Phys. F: Met. Phys. 16 (1986) 1161.
[53] A. Seeger, Phys. Lett. A 58A (1976) 137.
[54] M.H. McAdon, W.A. Goddard III, Phys. Rev. Lett. 55 (1985) 2563.
[55] M.H. McAdon, W.A. Goddard III, J. Phys. Chem. 91 (1987) 2607.
[56] M. Li, W.A. Goddard III, Phys. Rev. B 40 (1989) 12155.
[57] M. Li, W.A. Goddard III, J. Chem. Phys. 98 (1993) 7995.
[58] J. Kua, W.A. Goddard III, J. Phys. Chem. B 102 (1998) 9481.
[59] R. DiFoggio, R. Gomer, Phys. Rev. B 25 (1982) 3490.
[60] S.C. Wang, R. Gomer, J. Chem. Phys. 83 (1985) 4193.
[61] L.J. Lauhon, W. Ho, Phys. Rev. Lett. 85 (2000) 4566.
[62] Y. Hayashi, W.M. Shu, Diff. Defect Data–Solid State Data, Pt. B: Solid State Phenomena 73–75 (2000) 65.